A Mobile Robot: Sensing, Planning and Locomotion

David J. Kriegman
Ernst Triendl
Thomas O. Binford

Artificial Intelligence Laboratory
Stanford University
Stanford, CA 94305

ABSTRACT

A mobile robot architecture must include sensing, planning, and locomotion which are tied together by a model or map of the world based on sensor information, apriori knowledge and generic models. The architecture of a Stanford's autonomous mobile robot is described including its distributed computing system, locomotion, and sensing. Additionally, some of the issues in the representation of a world model are explored. Sensor models are used to update the world model in a uniform manner, and uncertainty reduction is discussed

1. Introduction

Stanford's autonomous mobile robot project is aimed at developing a vehicle that navigates within unstructured man made environments such as the inside of a building. To accomplish this goal, the robot must be able to sense its environment as well as move about within it.

The vehicle at Stanford is a testbed for a variety of sensors each with its own possibilities and limitations. Generally, one finds a tradeoff between resolution, accuracy, repeatability, and speed in sensing and processing; so no single form is adequate for all situations. The most flexible yet most costly sense, in terms of processing complexity, is computer vision. Vision affords a very detailed description of the environment. On a broader and coarser scale, ultrasonics are used to determine the presense of obstacles that the vision system may have overlooked. For closer proximity and protection, there is tactile sensing. The characteristics of these sensors must be modeled and their information must be intelligently integrated into a map or world model that is used for navigation and in the future, task planning.

2. System Architecture

The Stanford Mobile Robot [fig 1], known as the Mobile Autonomous Robot Stanford (MARS) or more affectionately, Mobi, is an omnidirectional vehicle (3DOF) with a novel three wheel configuration. The robot is essentially cylindrical with a diameter of 65cm and height of 170cm. The wheels, forming the edges of an equilateral triangle, have six contoured passive rollers along their chords, allowing the wheel to move sideways while driven. With a combination of driving the wheels about their major axis, and passive turning of the rollers, the vehicle can translate while simultaneously rotating. With this form of locomotion, the vehicle is well suited for indoor travel and maneuvering about tight obstacles. However, because of the small roller diameter, the vehicle is confined to traveling over relatively smooth terrain.

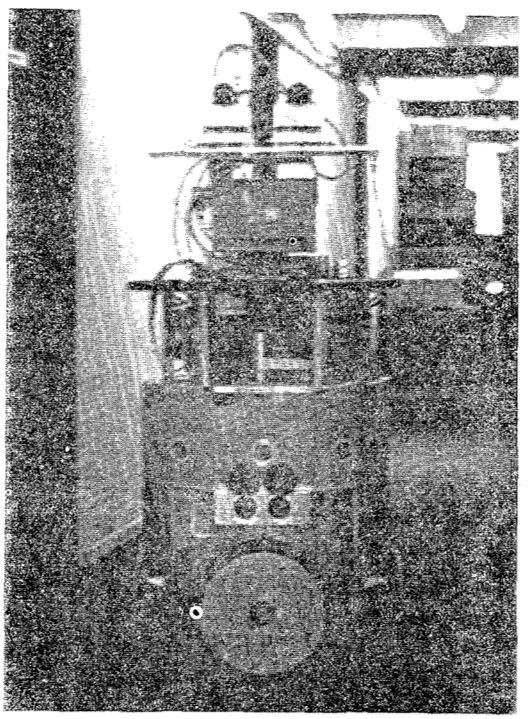

Figure 1. The robot

Each of the wheels' motor contains a shaft encoder that is used for odometry and trajectory following. Trajectories are specified by two systems: B-splines connect knot points to form a path with smoothly changing velocity. A second system, called Smooth Driver, connects straight line segments with clothoid curves to create trajectories that have continuous curvature and smooth acceleration along the path.[5]

Support for this work was provided by the Air Force Office of Scientific Research under contract F33615-85-C-5106, Image Understanding contract N00039-84-c-0211 and Autonomous Land Vehicle contract AIDS-1085S-1. David Kriegman was supported by a fellowship from the Fannie and John Hertz Foundation.

CH2413-3/87/0000/0402$01.00 © 1987 IEEE

The robot has four sensing modalities: vision, acoustics, tactile, and odometry. Stereo vision, using two onboard cameras, returns the 3 dimensional location of vertical lines within its field of view. and the details of this system can be found in [4]. The cameras are mounted on a pan/tilt head, giving them two degrees of freedom. The acoustic system is composed of twelve polaroid sensors equally spaced about the circumference of the robot. These sensors return a distance that is proportional to the time of flight of an echoed acoustic chirp. To a first approximation, the acoustics find the nearest object within a thirty degree cone. Though the acoustic system has very low angular resolution, it measures depth quite accurately making it useful for guarded moves. The information can also be incorporated into the world model as well as checking consistency of the existing model. As a last line of defense, if the vision and acoustic systems miss an object, there is a "tactile" sensing system, composed of twelve bumpers with internal tape switches. Besides emergencies, the information can augment the world model. Finally, the bumpers are useful for navigating through tight areas such as doorways where the edges of the door are within the minimum ultrasonic range and not within the region of stereo vision. Finally, odometry determines the robot's position.

The robot's computational system is distributed onboard and offboard, and figure 2 presents an overview of the architecture and subsystems. Onboard, a sixteen bit computer (National Semiconductor 32016) is responsible for trajectory planning, sensor data acquisition and communication. Because of the unnecessary burden of onboard program development, most of the intelligence is offboard, and so the onboard computer executes simple commands. Additionally, it handles real time emergencies such as stopping when a bumper is unexpectedly pressed (a crash).

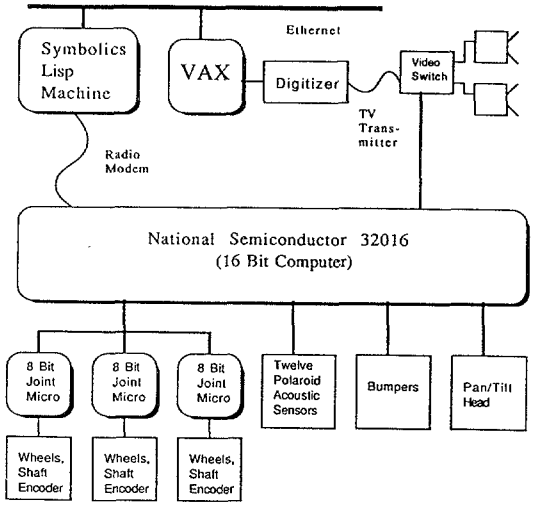

Figure 2. The robot's architecture

The robot communicates, via a digital radio link, with a (necessarily offboard) Symbolics Lisp Machine, which is responsible for planning operations such as sensor interpretation (except vision), sensor fusion, uncertainty reduction, map making, and path planning. The lisp machine also graphically displays the robot's status, including position and sensor values. For safety, planning algorithms are developed and tested on a simulator. A TV transmitter sends the video signal from the cameras to the digitizer. From there the image is transferred, via DMA link, to a VAX which does the image processing and computes stereo correspondence points that are sent to the Lisp Machine over an ethernet.

3. World Model

A critical design issue is the representation of the map or world model. The map must richly describe the world without burdensome details. Consider the purpose of a map. Generally, a mobile robot must reach the location needed to perform a task (e.g. getting my coffee cup from my desk). Without a map the robot could search all of the offices in my building and check for coffee cups using a straight forward search algorithm. Instead, the map can be searched for my room and then the robot can go there and look for the coffee cup.

Since the cost of a graph search is O(n), keeping the map small will speed search. An alternative to a small map, is a hierarchical representation so the search will be over a smaller map at each level of the hierarchy.

To make robots more useful, the robot should build the maps, not the person. Thus, the map is built bottom up, and the lowest level of information is closest to the actual sensor measurement while higher levels of the hierarchy become more abstract and symbolic. Figure 3 shows the hierarchy of objects that might describe a hallway in a building. At the lowest level are the points and lines found from the sensor information. This information is fit to a model of generic objects such as walls, doors, and windows. Two parallel walls that bound an elongated region of free space could be a hall, and hallways are found in buildings. So, when searching for a route between rooms in a building, we would search at the building level for route and then find paths along successive levels of the map.

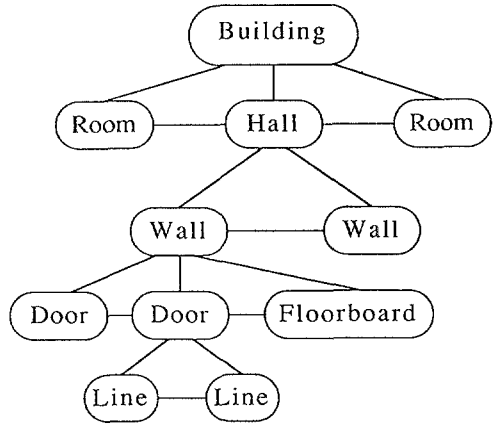

Figure 3. Hierarchical model

Another issue is whether to represent the world as 2 or 3 dimensional. Since our robot is confined to the indoors and only travels on fairly flat level surfaces, a 2-D coordinate frame represents robot location. However, the robot observes objects that are not confined to lie on the floor, and their location is in 3 dimensions.

Furthermore all sensing modalities posses some degree of uncertainty in measurement Because the inferred location of an object sensed from two distinct locations would be different without considering uncertainty, this must be represented, and so the map cannot be a grid based on an absolute coordinate system but must express the relationship of points to one another[6]. So, sensor data and their interpretation are represented relative to the location of the robot and the map becomes stretchy. Since the map cannot be based on a grid, hierarchical grid systems such as quad-trees are inappropriate.

A final issue is uncertainty representation. Uncertainty manifolds have been proposed where the actual value of a measurement is within a bounded region[6]. When determining the uncertainty of a sequence of motions, for example, the bounding manifold of the convolution of the individual manifolds is used. This has the unfortunate property of being overly conservative. Instead of using the bounding region, we describe measurements by a normal distribution (Gaussian), retaining the first two moments of the measurement probability density function (i.e mean vector, $\vec{\mu}$ and covariance matrix, Σ). All sensor data is gathered at discrete locations, and for each sensing, we create a Frame, F_i which is a local coordinate system with the robot at the origin. This frame is related to the previous frame, F_{i-1} by a transformation $\vec{T}_{i-1,i} = (x_i y_i \phi_i)^T$ which has a mean vector and covariance matrix. Additionally, each sensor reading S_j is related to the frame where the reading was taken. An example of these relationships is shown in figure 4. Locations are drawn as ellipses because ellipsoids are the equi-probability density contours of a multivariate normal distribution. The larger the ellipse, the greater the uncertainty.

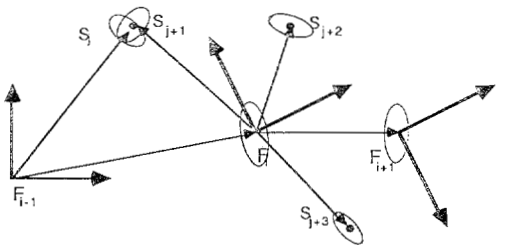

Figure 4. Relationship of frames and sensor readings

Uncertainty can be propagated or compounded[3]. For example if we know $\vec{T}_{i-1,i}$ and $\vec{T}_{i,i+1}$ we can determine the mean and covariance matrix of $\vec{T}_{i-1,i+1}$. Additionally, the uncertainty of the location of a point can be reduced if the point was sensed from two different frames. In figure 4, the point described by S_j and S_{j+1} are the same, and we can get tighter bounds on this location as well as the relationship between F_{i-1} and F_i.

4. Sensor Models

The mobile robot receives information about its environment from its shaft encoders, contact bumpers, ultrasonics, and stereo vision. This information has some common characteristics (e.g. spatial location of objects) and some unique characteristics (e.g. vision can give the color of an object). The fundamental measurement that all of these sensors yield is the position of an object, s_i. which is described by a multivariate normal probability density function with mean vector $\vec{\mu}_{s_i} = (\mu_{x_i} \mu_{y_i} \mu_{z_i})^T$ and covariance matrix

$$\Sigma_{s_i} = \begin{pmatrix} \sigma_{x_i x_i} & \sigma_{x_i y_i} & \sigma_{x_i z_i} \\ \sigma_{x_i y_i} & \sigma_{y_i y_i} & \sigma_{y_i z_i} \\ \sigma_{x_i z_i} & \sigma_{y_i z_i} & \sigma_{z_i z_i} \end{pmatrix} \quad (1)$$

and so the probability that a sensed point s_i is at $\vec{x}$ is:

$$f_{s_i}(\vec{x}) = \frac{e^{-\frac{1}{2}(\vec{x}-\vec{\mu})^T \Sigma^{-1} (\vec{x}-\vec{\mu})}}{2\pi\sqrt{|\Sigma_i|}} \quad (2)$$

4.1 Robot Motion

As the robot moves, shaft encoder readings, $\vec{\varphi}$, are mapped through the kinematics, K, to determine robot velocity and integrated to calculate vehicle location. So the motion is

$$\vec{p} = \int_{t_0}^{t} K(\frac{\partial \vec{\varphi}}{\partial t}) dt \quad (3)$$

After the robot has moved far enough a frame is created and related to the previous one by a transformation described by a normal random vector, $\vec{T}_i = (x_i y_i \phi_i)^T$,

When our robot moves, it is generally accurate in distance traveled but its orientation can be off by a few degrees. This leads to fairly large Cartesian errors in the orthogonal direction to the travel direction. Analogously, when a flagpole moves in the wind, its height will not change drastically, but the top of the pole may move parallel to the ground by many feet. Thus for a commanded straight line motion of:

$$\Delta\vec{P} = \begin{pmatrix} \Delta x \\ \Delta y \\ \Delta\phi \end{pmatrix} = \begin{pmatrix} \Delta r cos\Delta\theta \\ \Delta r sin\Delta\theta \\ \Delta\phi \end{pmatrix} \quad (4)$$

the mean, μ_p is computed by equation 3, and in the direction of motion, the covariance matrix of the uncertainty in position is

$$\Sigma_r = F(\Delta r, \Delta\phi) \quad (5)$$

Σ_r can be rotated by θ yielding Σ_p. Thus, the transformation between two successive frame is described by μ_p and Σ_p.

4.2 Bumpers

The mobile robot has twelve bumpers with internal contact switches along the edges of a nonregular Dodecagon. In addition to protection when the robot accidently crashes, the bumpers provide very definite information about the presence and location of an object; this information can be added to the map. If we assume that we only contact one object (i.e. either a corner or wall) at a time, then the geometry of the bumpers allows us to make the following interpretations.

a. If two adjacent bumpers are contacted as in figure 5a, then the contact was in the corner and we can localize the contact point to that corner with a fairly high degree of certainty. Additionally, if that point is part of a wall, we have a bounds on wall direction relative to the robot.

b. If only one bumper is contacted, [fig 5b], then the point of contact is a uniform distribution along the length and depth of the bumper.

c. Finally, if the contact is with three adjacent bumpers [fig 5c] then the contact is planar, and the direction of contact is that of the central bumper with an uncertainty based on the depth of the bumpers.

These interpretations have been used for passing through doorways where there is only one contact at any time.

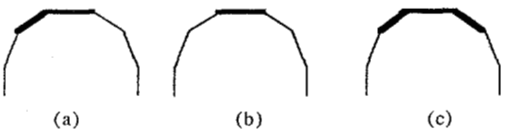

Figure 5. Bumper contacts:
(a) corner of robot contacts a corner or plane,
(b) bumper contacts a corner
(c) bumper contacts a plane

4.3 Ultrasonics

Currently, twelve Polaroid ultrasonic sensors [2] surround the robot, and provide direct range information at 10 readings per second. The sensing rate is due to the speed of sound and time required for a previous chirp to be attenuated by air. From experimentation, which has been confirmed by others[1], we have found that the system is sensative over approximately 30°. This rather wide spread is one of the complications of using ultrasonics because it tends to blur edges and corners. The other major drawback are specularities due to the large acoustic wavelength, ($\sim$ .6cm). Many objects have surfaces that are smooth compared to the acoustic wavelength causing the transmitted sound to be specularly reflected, and so the nearest object may not cause the first echo.

Figure 6 shows an overhead view of a portion of a hallway and figure 7 presents a rotational scan of the hallway at five degree increments with five readings taken at each position. The lines represent the sensor's central axis, and the distance from the inner end-point of the lines to the circles on that line are the distances of the each sonar reading. Some of the interesting observations about this scan are noted below and are marked by letters in the figure and text.

First there is small amount of noise on each sensor reading (a) which leads to a rather tight distribution of distances especially when the echo is strong such as when the axis of the sensor is close to the normal of the surface. This uncertainty can be easily modeled as a Gaussian stochastic process. Straight lines can be readily extracted to determine the position and direction of the wall as in (b) using a least mean square best line fit. This has been previously applied to a wall following algorithm. Also specularities are seen at some angles due to the smoothness of the walls at larger grazing angles as point (c) shows. Note that a specular reflection off of the near wall and then a good back reflection by the far wall causes this reading. Point (d) shows a reading where there were actually reflections off both walls. In the direction down the hall (e) shows that larger variation in the sensor readings due to the larger distances and angles of incidence with all surfaces.

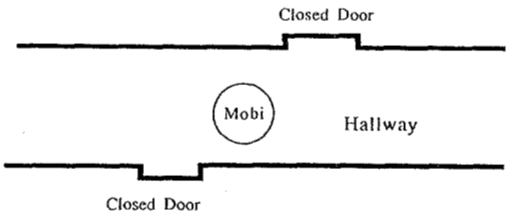

Figure 6. Overhead view of the hallway

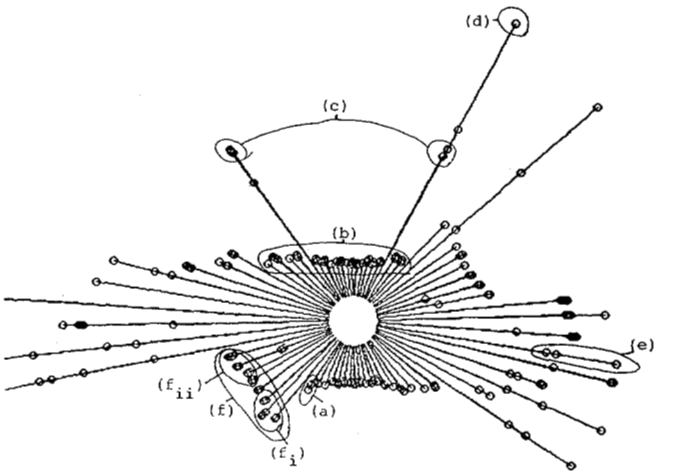

Figure 7. Sonar scan of the hallway in previous figure

A final interesting point to note is (f) which is caused by the corner of a closed door and its molding. The doors are very smooth and quite specular so even at moderate incidence angles, there are reflections. However, the door edge is slightly recessed (7 cm) and this causes a dihedral where any ultrasonic energy that is close enough to the corner will be specularly reflected off one edge and then reflected by the second edge, leaving in the same direction

as the incoming chirp as shown in figure 8. Because the reflections occur over the entire length and width of the dihedral, a very strong echo is received. Given that there are no objects closer than the Dihedral, the width of the apparent dihedral will be on the order of the sensor beam width as shown by the points highlighted in (f_{ii}). Note that a corner such as a post will also yield the same width reading however the echo will not be nearly as strong. The readings in (f_i) are interesting because the acoustic chirp's first point of contact is the door, but this is specularly reflected, and the dihedral causes the first returned echo.

After a scan such as figure 7 we can extract straight line segments such as were highlighted by (b) If its length is on the order of a beam width such as the one extracted by (f), then there are two possible interpretations, either a straight line or a corner (dihedral). Additionally, these straight line readings inform us that the region between the robot and the segment is free space. The consistency of these features with the map can be ascertained, and the map can be updated. Additionally, based on the extracted straight lines and the world model, specularities such as points (c) and (d) can be found. Finally, those readings that can not be modeled as straight lines or corner points can be added to the map as representing a surface patch that could lie anywhere along 30° arc. Because the surface patch causing the echo is more likely near the axis of the sensor[1], and to make the representation more uniform with other point locations, a chord approximates the arc, and the location is represented as a normal distribution. The patch's mean is along the sensor axis, and there is a large variance along the chord and a small variance in the direction of the sensor axis.

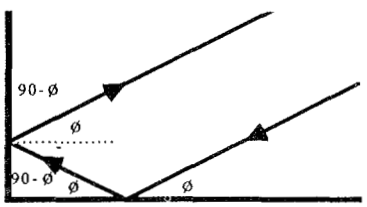

Figure 8. Acoustic reflections in a dihedral

4.4 Vision

The stereo vision system described in [4] locates vertical edges in space. These are incorporated into the map as extending down to the ground plane and upward to the ceiling, and so only the (x,y) location is of concern. As with the other sensor measurements, there is uncertainty in the location of the vertical which we describe by a normal distribution with a mean vector of $\vec{\mu} = (\mu_x \mu_y)^T$ and a covariance matrix:

$$\Sigma = \frac{4d^2}{(\mu_{x_r} - \mu_{x_l})^4}\sigma^2 \begin{pmatrix} \mu_{x_l}^2 + \mu_{x_r}^2 & -f(\mu_{x_r} + \mu_{x_l}) \\ -f(\mu_{x_l} + \mu_{x_r}) & 2f^2 \end{pmatrix} \quad (6)$$

where μ_{x_l} and μ_{x_r} are the locations of the edges in the left and right images. σ^2 is the variance in the location of image vertical, f is the focal length of the lenses and $2d$ is the stereo baseline. This has been derived in Appendix A. Figure 9 shows the resulting error ellipses of a stereo image looking down the hallway. The ellipses grow quickly in length with respect to the mean distance, becoming long and narrow. Also, notice the one large nearby ellipse caused by poor localization of a low resolution edge.

Stereo correspondence points are generally the most accurate form of sensed measurement available. Of course, one must consider that stereo has a high computational cost and only covers a rather narrow field of view. An interesting point is that at even moderate distances, the uncertainty in distance measurement from stereo becomes larger than angular uncertainty which is complementary to the acoustics that have broad angular resolution and good depth accuracy.

Figure 9. Stereo correspondance points in a hallway from a single position

5. Reducing Motion Uncertainty

Generally, it is important to be able to recognize that two observed points are either the same or part of the same structure. If they are the same, then they will have similar characteristics (e.g. color, grey level gradient) as well as proximity as measured from two different frames. Additionally, points must be aggregated to instantiate a model. This can be more easily accomplished if uncertainty is reduced. From experience, we have found the most influential source of uncertainty when fusing information from different scenes is the motion transform between them. Furthermore, uncertainty is compounded across multiple transforms, so aggregating points between views that are a large distance apart becomes more difficult; thus, uncertainty in odometry must be reduced.

Uncertainty can reduced by applying a Kalman filter to the sensor information and this is explained through an example using stereo vision as the sensor in Figure 10. Consider, (in fig 10a) the uncertainty ellipses of two points (C_a and C_b), determined from equation 6, that were viewed from two different locations, (P_1 and P_2). This figure shows that there was an error in motion transform, $T_{1,2}$ as determined by odometry because correspondence points C_{a_1} and C_{a_2} should be coincident as should C_{b_1} and C_{b_2}. Given the uncertainty in robot location, P_2, which is determined from equations 4 and 5, and represented by the ellipse about its mean in fig. 10b. The uncertainty in the location of the stereo points C_{a_2} and C_{b_2} with respect to location P_1 are found by compounding [3], also shown in fig. 10B. Correspondence between vertical edges from two successive

stereo views can be determined by using the edge characteristics. In this case $C_{a_1} \equiv C_{a_2}$ and $C_{b_1} \equiv C_{b_2}$, so we can apply a Kalman filter to reduce the uncertainty in the stereo correspondences and motion transform. The transform and the correspondence points as seen from P_1 become our initial state vector along with their covariances. The stereo measurements as well as the transform are assumed to be independent. The correspondence points as seen from P_2 becomes the measurement vector, and the Kalman filter[10] is applied to obtain a better estimate of the state as shown in figure 10c. Note that the motion uncertainty has been reduced as has the location of the correspondence points as viewed from both positions.

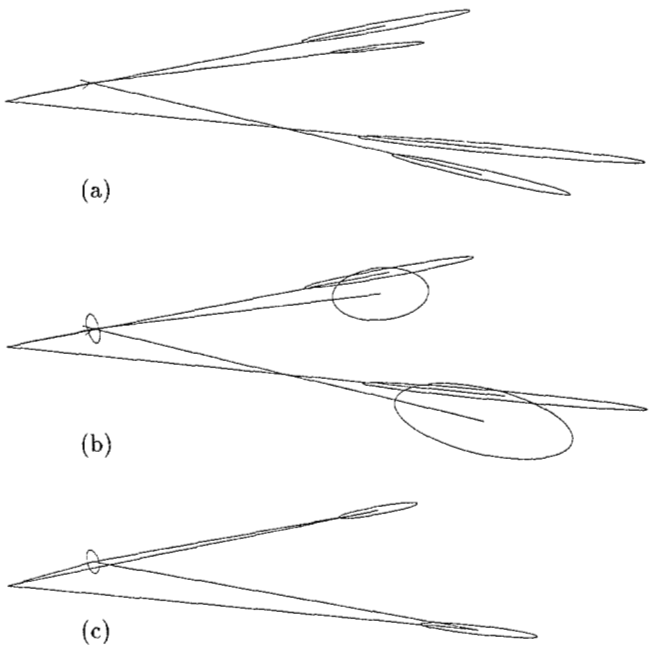

Figure 10. Uncertainty reduction, merging two views:
(a) Two points seen form different locations
(b) Uncertainty with respect to P_1
(c) Uncertainty reduced

This technique can be used to integrate motion sequences and build models from multiple views. Figure 11a shows a motion sequence composed of correspondence points found from eight positions. The scale is 1 meter, and the shape of the mark of the correspondence and the mark at the center of the robot indicates the robot's position when sensing that point. In this figure, the robot's location was determined purely by odometry. Between each successive location, motion correspondences were determined along with the error models of odometry and stereo. The Kalman filter was applied, and the points in figure 11b form the two walls of a hallway, demonstrating that motion uncertainty was greatly reduced. The circles were seen only once while the squares depict merged points. The observant reader will notice that one of the correspondence points is touching mobi's perimeter; Mobi crashed in this run.

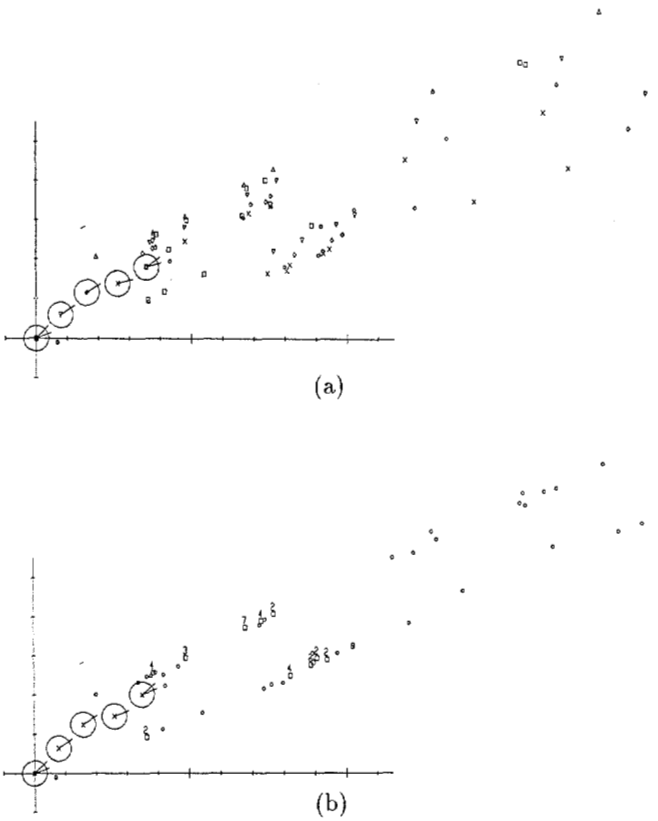

Figure 11. Motion sequence:
(a) Location of correspondence points with odometry determing the robot's location
(b) Location of the same points after kalman filter was applied

6. Conclusions

We have presented the architecture of Stanford mobile robot and described the modeling of information from the four sensor sources, stereo vision, acoustics, bumpers and odometry. This information is used to update a world model whose hierarchical representation ranges from symbolic information to sensor data. All locations in the world model are relative to other points and measurement uncertainty is explicitly represented by multivariate normal distributions. Uncertainty can be reduced by applying a Kalman filter to the data and has been applied to reducing motion uncertainty.

Appendix A. Derivation of Uncertainty in Stereo

Given a stereo vision system of two cameras with parallel image planes and horizontal epipolar lines, the uncertainty in the location of stereo correspondence point can be found (equation 7). Consider the overhead view of the stereo arrangement in figure 12 during this derivation. Only the projection onto the ground plane is considered. Given the

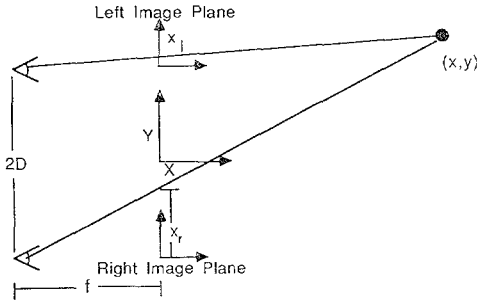

Figure 12. The stereo setup

focal length of the cameras, f, the baseline distance, $2d$ between cameras, and the location of the points in the image plane, x_l and x_r, which are described by a normal distribution. Thus, the location of a point in the image is given by a mean μ_{x_i} and variance $\sigma_{x_i x_i}$. From [7] we know that the location of the point in space is:

$$\vec{x} = \begin{pmatrix} x \\ y \end{pmatrix} = \begin{pmatrix} F(x_l, x_r) \\ G(x_l, x_r) \end{pmatrix} = \begin{pmatrix} \frac{d(x_r + x_l)}{x_r - x_l} \\ f - \frac{2df}{x_r - x_l} \end{pmatrix} \tag{7}$$

Since a linear function of normal random variables is normal, nonlinear F and G are linearized about the mean of x_l and x_r with a Taylor Series expansion:

$$\begin{aligned} x \approx & F(\mu_{x_l}, \mu_{x_r}) + \frac{\partial F(x_l, x_r)}{\partial x_l}\Big|_{\substack{x_l=\mu_{x_l} \\ x_r=\mu_{x_r}}} (x_l - \mu_{x_l}) \\ & + \frac{\partial F(x_l, x_r)}{\partial x_r}\Big|_{\substack{x_l=\mu_{x_l} \\ x_r=\mu_{x_r}}} (x_r - \mu_{x_r}) \\ = & d\frac{\mu_{x_r} + \mu_{x_l}}{\mu_{x_r} - \mu_{x_l}} + \frac{2d\mu_{x_r}}{(\mu_{x_r} - \mu_{x_l})^2}(x_l - \mu_{x_l}) \\ & - \frac{2d\mu_{x_l}}{(\mu_{x_r} - \mu_{x_l})^2}(x_r - \mu_{x_r}) \end{aligned} \tag{8}$$

and similarly.

$$\begin{aligned} y \approx f - \frac{2df}{\mu_{x_r} - \mu_{x_l}} & - \frac{2df}{(\mu_{x_r} - \mu_{x_l})^2}(x_l - \mu_{x_l}) \\ & + \frac{2df}{(\mu_{x_r} - \mu_{x_l})^2}(x_r - \mu_{x_r}) \end{aligned} \tag{9}$$

Now, the Jacobian, J, of the transform is:

$$J = \begin{pmatrix} \frac{\partial x}{\partial x_l} & \frac{\partial x}{\partial x_r} \\ \frac{\partial y}{\partial x_l} & \frac{\partial y}{\partial x_r} \end{pmatrix} = \begin{pmatrix} \frac{2d\mu_{x_r}}{(\mu_{x_r} - \mu_{x_l})^2} & \frac{-2d\mu_{x_l}}{(\mu_{x_r} - \mu_{x_l})^2} \\ \frac{-2df}{(\mu_{x_r} - \mu_{x_l})^2} & \frac{2df}{(\mu_{x_r} - \mu_{x_l})^2} \end{pmatrix} \tag{10}$$

so the mean of the location of the point in space is determined from equation 7:

$$\vec{\mu} = \begin{pmatrix} \mu_x \\ \mu_y \end{pmatrix} = \begin{pmatrix} F(\mu_{x_l}, \mu_{x_r}) \\ G(\mu_{x_l}, \mu_{x_r}) \end{pmatrix} \tag{11}$$

and the covariance is:

$$\Sigma = \begin{pmatrix} \sigma_{xx} & \sigma_{xy} \\ \sigma_{xy} & \sigma_{yy} \end{pmatrix} = J \begin{pmatrix} \sigma^2_{x_l} & 0 \\ 0 & \sigma^2_{x_r} \end{pmatrix} J^T \tag{12}$$

and assuming that $\sigma^2_{x_l} = \sigma^2_{x_r} = \sigma^2$ then the covariance matrix of a stereo correspondence point is:

$$\Sigma = \frac{4d^2}{(\mu_{x_r} - \mu_{x_l})^4}\sigma^2 \begin{pmatrix} \mu^2_{x_l} + \mu^2_{x_r} & -f(\mu_{x_r} + \mu_{x_l}) \\ -f(\mu_{x_l} + \mu_{x_r}) & 2f^2 \end{pmatrix} \tag{13}$$

Acknowledgements

We'd like to thank Soon Yau Kong, Ron Fearing, Giora Gorali, Shaul Fishman and Joel Burdick, for all their help and suggestions.

References

[1] Moravec, HP; Elfes, A., "High Resolution Maps from Wide-Angle Sonar," Proceedings IEEE International Conference on Robotics and Automation, 1986.

[2] "Ultrasonic Ranging System," Commercial Battery Division, Polaroid Corp, Cambridge, MA, 1984.

[3] Smith, Randall; Self, Matthew; Cheeseman, Peter, "Estimating Uncertain Spacial Relationships in Robotics," Proceeding AAAI Workshop on Uncertainty in Artificial Intelligence, August, 1986.

[4] Triendl, Ernst; Kriegman, David, "Stereo Vision and Navigation within a building," 1987 IEEE conference on Robotics and Automation.

[5] Kanayama, Yutaka; Miyake, Norihisa, "Trajectory Generation for Mobile Robots," Third International Symposium of Robotics Research, Gouvieux, France, 1985.

[6] Brooks, Rodney A., "Visual Map Making for a Mobile Robot," Proceedings IEEE International Conference on Robotics and Automation, St. Louis, 1985.

[7] Ballard, Dana H., Brown, Christopher M., "Computer Vision," Prentice-Hall, inc. Englewood Cliffs, New Jersey, 1982.

[8] Chatila, Raja; Laumond, Jean-Paul, "Position Referencing and Consistent World Modeling for Mobile Robots," Proceedings of the 1985 IEEE International Conference on Robotics and Automation, St. Louis, 1985.

[9] Flynn, Anita M., "Redundant Sensors for Mobile Robot Navigation," MIT AI-TR 859, 1985.

[10] Kailath, T., "Lectures on Wiener and Kalman Filtering," Springer-Verlag, 1981.